Activation of Nod2 signalling upon Norovirus infection enhances antiviral immunity and susceptibility to colitis

Ghaffar Muharram, Marion Thépaut, Pierre-Emmanuel Lobert, Teddy Grandjean, Olivier Boulard, Myriam Delacre, Emmrich Wakeford, Richard Wheeler, Lionel Franz Poulin, Ivo Gomperts Boneca, et al.

Activation of Nod2 signalling upon Norovirus infection enhances antiviral immunity and susceptibility to colitis

Authors: Ghaffar Muharram[a], Marion Thépaut[a], Pierre-Emmanuel Lobert[c], Teddy Grandjean[a], Olivier Boulard[b], Myriam Delacre[a], Emmrich Wakeford[a], Richard Wheeler[e], Lionel Franz Poulin[b], Ivo Gomperts Boneca[e], Frank Lafont[a], Marie-Cécile Michallet[d], Didier Hober[c], Ken Cadwell[f,g,h], Mathias Chamaillard[b].

Affiliations :

[a]Univ. Lille, CNRS, Inserm, CHU Lille, Institut Pasteur de Lille, U1019 - UMR 9017 - CIIL - Centre d'Infection et d'Immunité de Lille, F-59000 Lille, France.

[b]Laboratory of Cell Physiology, INSERM U1003, University of Lille, Lille, France.

[c]Univ Lille, Faculté de Médecine, CHU Lille, Laboratoire de Virologie ULR3610, Lille, France.

[d]TERI (Tumor Escape, Resistance and Immunity), Centre de recherche en cancérologie de Lyon, Centre Léon Bérard, Université de Lyon, Université Claude Bernard Lyon 1, Inserm 1052, CNRS 5286, 69008 Lyon, France.

[e]Institut Pasteur, Université Paris Cité, CNRS UMR6047, INSERM U1306, Unité de Biologie et génétique de la paroi bactérienne, F-75015, Paris, France

[f]Kimmel Center for Biology and Medicine at the Skirball Institute, New York University Grossman School of Medicine, New York, NY 10016, USA

[g]Department of Microbiology, New York University Grossman School of Medicine, New York, NY 10016, USA

[h]Division of Gastroenterology and Hepatology, Department of Medicine, New York University Langone Health, New York, NY 10016, USA

Disclosure of interest:

K.C. has received research support from Pfizer, Takeda, Pacific Biosciences, Genentech, and Abbvie; consulted for or received honoraria from Vedanta, Genentech, and Abbvie; and holds U.S. patent 10,722,600 and provisional patent 62/935,035 and 63/157,225.

Correspondence should be addressed to:

Mathias Chamaillard, PhD, Phone number: +33359317427, Fax number: +33359317480, E-mail: mathias.chamaillard@inserm.fr

Ghaffar Muharram, PhD, phone number: +33320871033, E-mail: ghaffar.muharram@pasteur-lille.fr

Key words: NOD2, Norovirus, Inflammation, Colitis, Macrophages, Signalling.

Data availability statement: the data that support the findings of this study are available from the corresponding author, GM or MC, upon request on HAL

Abstract. Over 90% of epidemic nonbacterial gastroenteritis are caused by human Noroviruses (NoV) which are persisting in a substantial subset of people allowing their spread worldwide. It leads to a significant number of endemic cases and up to 70,000 children deaths in developing countries. NoVs are primarily transmitted through the fecal-oral route. To date studies have focused on the influence of the gut microbiota on viral clearance by enteric immunity. In this study, the use of the persistent mouse Norovirus S99 strain (MNoV_S99) allowed us to provide evidence that the norovirus-driven exacerbation of colitis severity relied on bacterial sensing by nucleotide-binding oligomerization domain 2 (Nod2). Similarly, another persistent MNoV_CR6 strain failed to exacerbate colitis severity in Nod2-deficient mice. In parallel, the viremia was heightened in these mice in comparison with control animals. Accordingly, a reduced level of phosphorylation of Signal Transducer and Activator of Transcription1 (STAT1) in Nod2-deficient macrophages infected by MNoV_S99 was measured. By contrast, STAT1 phosphorylation was increased in wild-type macrophages and associated with an induction of NOD2 expression. This in turn enhances myeloid cells response to muramyl dipeptide (MDP) resulting in downstream pro-inflammatory cytokine secretion and reduced noroviral production. Hence, our results uncover a previously unidentified virus-host-bacterial interplay that may represent a novel therapeutic target for treating noroviral origin gastroenteritis that may be linked with susceptibility to several common illnesses such as Crohn's disease.

Introduction. With the development of high throughput sequencing techniques, we are progressively gaining a better knowledge of the composition of the enteric virome (ensemble of gut virus communities)[1]. This is of particular importance for unravelling how some enteric viruses can establish persistent infections and the subsequent consequences on health[2,3]. Amongst enteric viruses yielding pro-inflammatory phenotypes, noroviruses (NoV) are responsible for the majority of non-bacterial gastroenteritis worldwide. These single stranded RNA (+) viruses, belonging to the family of *Caliciviridae* have been studied for several years. Until recent progress in cultivation methods of noroviruses from genogroups I, II, IV, VIII and IX[4–6] that infect humans (HuNoVs), mechanistic details were mostly obtained from studies using the mouse norovirus (MNoV)[7]. Indeed, MNoVs can be easily produced *in vitro* in macrophages or dendritic cells[8]. Several MNoV strains have been described based on their shedding time in the stool and classified as persistent or acute (non-persistent) strains[9].

Multiple intracellular pattern recognition receptors (PRR) have been associated with indirect noroviral detection, especially during NoV genome replication, when double stranded RNA intermediates are generated[10]. The Toll like receptor 3 (TLR3) that recognizes any dsRNA in the endosomal compartment and the melanoma differentiation associated protein-5 (MDA-5), a member of the RIG-I like receptor (RLR) family that recognizes long dsRNA, have been shown to participate in the detection of the MNoV_1 strain and its plaque isolate the MNoV_CW3[11]. Amongst the Nod like receptor (NLR) family, Nlrp6 was shown to bind with the encephalomyocarditis virus (EMCV), a single strand RNA (+) enteric virus, via the RNA helicase Dhx15. Following the formation of these complexes, interferon (IFN) type I and III signalling responses are triggered via the recruitment of the mitochondrial antiviral signalling (MAVS) protein. Interestingly, this study also showed that, Nlrp6$^{-/-}$ mice infected with MNoV_1 had higher viremia, suggesting similar mechanisms of NoV sensing by Nlrp6[12]. Another member of the NLR family, the nucleotide-binding oligomerization domain 2 (NOD2)

mostly known as a sensor of muropeptides from Gram positive and negative bacteria[13], was also shown to directly bind with the genome (ssRNA-) of the respiratory syncytial virus (RSV) to induce antiviral responses[14]. The recruitment of MAVS by NOD2 was needed to activate the interferon-regulatory factor 3 (IRF3) dependent signalling and provoke IFN-β production. In the same line, NOD2 dependent signalling was shown to potentiate gut inflammation and increase lethality in an *E. Coli* and MNoV_1 co-infection mouse model[15].

Another molecular player that is essential to activate antiviral signalling is the cytosolic protein signal transducer and activator of transcription 1 (STAT1). MNoV_1 infections were shown to be lethal in STAT1 knock-out mice[16]. Furthermore, STAT1 dependent interferon responses were shown to limit MNoV_1 replication and dissemination *in vivo*[17].

Owing to the variety of circulating NoV strains, strain-dependent effects are expected to occur and should be studied more in details. Even a single amino acid change in the NS1/2 viral protein is sufficient to switch the acute MNoV_CW3 strain to a persistent state[18], showing the high degree of adaptability of NoV genomes and hence their versatility to counteract host defence mechanisms. Type III interferon (IFN-λ) response has been shown to control the *in vivo* propagation of the persistent MNoV_CR6 strain[19], while type I and II interferons mediate innate immune responses against acute MNoV infections[16,20].

Interestingly, Cadwell and colleagues have demonstrated how infection with the MNoV persistent strain CR6 rendered *Atg16l1*^{HM} mice more susceptible to dextran sodium sulphate (DSS)-induced colitis[21]. Interestingly, NOD2's interaction with ATG16L1 was shown to regulate the autophagy clearance of pathogenic bacteria[22]. Indeed, improper interaction with muropeptides and other metabolites from the gut microbiota leads to intestinal inflammation[23] and loss-of-function point mutations of either *NOD2* or *ATG16L1* predispose humans to Crohn's disease[24,25]. Insights into the mechanisms of how NOD2 signaling is regulated upon

noroviral infection and whether it may subsequently modulate colitis susceptibility remained to be assessed.

In this study, we have investigated the underlying mechanism of the pathogenesis of two persistent MNoV strains, namely S99 (*Berlin*)[26] and CR6. MNoV_S99 dependent inflammatory response to DSS was compared in WT and *Nod2*$^{-/-}$ mice. Similarly, the consequences of infections with MNoV_CR6 on disease risk were assessed in WT, *Nod2*$^{-/-}$ and *Atg16l1*^{HM} *mice*. Nod2-dependent pro-inflammatory signalling pathways activation were further examined in response to MNoV_S99 infection in myeloid cells to determine how this in turn may affect viral production.

Results.

MNoV_S99 exacerbates the DSS-induced inflammation

Since MNoV_S99 is a natural strain commonly found in animal facilities that is able to establish persistent infections[26], we assessed MNoV_S99's implication in the vulnerability to exacerbated inflammatory responses of the intestinal mucosa. Hence, we examined MNoV_S99's impact in a widely used chemically-induced colitis model that is induced upon administration of Dextran Sodium Sulfate (DSS). Specifically, C57BL/6J mice were first infected with a single dose of 10^7 $TCID_{50}$PFU of MNoV_S99 or mock-treated with PBS. One week later, drinking water was replaced with either a 3% DSS or 5% DSS solution for a period of seven consecutive days (Fig. 1A). Body weight-loss was monitored on a daily basis together with signs of diarrhea and rectal bleeding. With both concentrations of DSS, the pre-treatment with MNoV_S99 had induced a more significant body weight loss (purple and orange curves Fig. 1B and C). After 7 days of DSS treatment, mice were euthanized. Histological analysis of colon sections revealed an increased infiltration of inflammatory cells and epithelial damage in

infected mice treated with DSS when compared to similarly challenged animals that were not infected (Fig. 1D). Next, we quantified the muscle thickness from these colon sections. An increased thickness was measured in mice treated with the virus in presence of both 3 and 5% DSS in comparison with Mock-treated control mice (Fig. 1E). Similarly, histological scoring of the haematoxylin and eosin (H&E) stained colonic sections expectedly showed significantly more severity in mice treated with MNoV_S99 + 3% or 5% DSS than DSS alone (Fig. 1F). Upon mice sacrifice, resected colons were measured. A significantly reduced length was obtained in mice infected with MNoV_S99 and treated with 5% DSS in comparison with non-infected control animals (PBS) (Fig. 1G). The increased level of colitis was also evidenced by a significantly augmented secretion of the pro-inflammatory cytokine interleukin-6 (IL-6) in the supernatants of over-night *in vitro* cultured colon explants from MNoV_S99 infected + 5% DSS treated mice versus those from DSS only mice (Fig. 1H). Taken together, these data clearly show a much worse inflammation state in mice infected with MNoV_S99 in our chemically induced colitis model.

MNoV_S99 associated inflammation is abrogated in *Nod2*$^{-/-}$ mice

In cells from the myeloid lineage, NOD2 was shown to participate in the sensing of *Citrobacter rodentium* and of commensal bacteria that are translocating in response to chemically-induced epithelial injury[27]. To determine whether NOD2 is also implicated in the immunopathology of MNoV in our preclinical model of colitis, we compared the severity of DSS-induced colitis in the presence of MNoV_S99 or not between WT and *Nod2*-deficient mice. In contrast to what was observed in WT mice (Fig. 2A), the sensitizing effect of the virus on the daily weight-loss was absent upon MNoV_S99 infection of *Nod2*$^{-/-}$ mice (Fig. 2B). These data suggest that the pro-inflammatory effect of MNoV_S99 observed in WT mice is a consequence of a loss of tolerance to bacterial MDP. Indeed, DSS induces an abrasion of the epithelial barrier allowing

commensal bacteria to cross the mucosa and unleash a pro-inflammatory response from *Nod2* expressing cells. This was further confirmed after mice were autopsied. Colon tissue sections staining confirmed the decreased levels of colonic inflammation from MNoV_S99 infected *Nod2*$^{-/-}$ vs WT mice (Fig. 2C). In agreement, muscle thickness quantification from these colon sections showed significantly increased thickness in MNoV_S99-infected WT mice under 3% DSS treatment vs 3% DSS alone (Fig. 2D). While in *Nod2*$^{-/-}$ mice subjected to similar conditions, the excess of inflammation caused by the viral infection was lost. Consequently, the variations of colon length measurements that were induced upon MNoV_S99 infection were absent in *Nod2*$^{-/-}$ mice when compared to WT infected mice (Fig. S1A). Similarly, differences in histological scores measured from MNoV_S99-infected WT mice vs DSS alone were also lost in *Nod2*$^{-/-}$ infected mice (Fig. S1B). And a clear trend was observed regarding the increased levels of secretion of Tumour necrosis factor α (TNFα) in the supernatants of *in vitro* cultured colon explants from WT mice infected with MNoV_S99 and treated with 3% DSS vs those with DSS only. This effect was absent in the supernatants from *Nod2*$^{-/-}$ mice infected and treated similarly (Fig. S1C).

Overall, these data show the importance of bacterial sensing by NOD2 and the excessive inflammatory response measured in the presence of MNoV_S99 in our DSS-induced colitis mouse model.

Mouse noroviruses infections triggers NOD2-dependent pro-inflammatory signalling

Mouse noroviruses are known to have a tropism for the myeloid cell lineages, namely macrophages and dendritic cells. Recently it was shown that Tuft cells belonging to the gut epithelial cellular lineages, that possess the CD300lf MNoV receptor can also be targeted by the MNoV_CR6 strain[28].

202 Making use of the GFP-Nod2 reporter mice line, we first examined in which cellular lineages
203 Nod2 is expressed. We failed to observe GFP-Nod2 expression in epithelial cells, while plenty
204 of signal was detectable in the bulk of the cells below the lamina propria where myeloid cells
205 are located (Fig. 3A). Hence, our investigations regarding NOD2 expression variations in
206 response to MNoV_S99 infection focused on macrophages, monocytes and dendritic cells in
207 our *in vitro* cellular models.
208 Interferon production being one of the most common response to the intracellular presence of
209 RNA genomes of foreign origin, we examined if the STAT1 signalling pathway that lays
210 upstream of ATG16l1-mediated interferon production was activated in response to murine
211 norovirus infection.
212 To this end, bone marrow derived macrophages (BMDM) from WT mice were infected with
213 several MNoV strains at a multiplicity of infection (Moi) of 1, for 1h and pSTAT1 levels of
214 expression from cell lysates were measured by western blot (Fig. 3B). In contrast to the non-
215 persistent strain MNoV_CW3 that caused a striking increase in pSTAT1 level, the persistent
216 strains S99 and CR6 infections induced a much milder STAT1 signalling pathway activation.
217 The CW1 strain was associated with the lowest level of activation. Since MNoV_S99 is a
218 natural strain commonly found in animal facilities that is able to establish persistent infections,
219 we further analysed the mechanistic details behind its infection in our cellular models.
220 Using the macrophage cell-line Raw264.7, we confirmed that MNoV_S99 is able to induce
221 phosphorylation of STAT1 (Tyrosine 701) at different times at Moi 1 (Fig. S3). pSTAT1 was
222 detectable as early as 15 minutes post-infection and its expression further increased at 30 min
223 and 1h, while total STAT1 was detectable in control non-infected cells and its expression only
224 slightly increased at later time-points. In addition to the STAT1 activation through the Janus
225 kinases JAK1 and Tyk2, we also examined the status of NFκB activation, another pro-
226 inflammatory signalling pathway. For this purpose, pIκBα levels were quantified from infected

227 cell lysates. Despite basal low-level activation in mock-infected cells, pIκBα intensity increased
228 slightly at 30 min and 1h post-infection. However, no significant increase was measured. When
229 checking PI3K-AKT or the MAPK-ERK signalling axes in the same time frame, MNoV_S99
230 failed to induce any activation of these signalling pathways (Fig. S2). Next, we analyzed the
231 response of BMDM derived from WT or *Nod2*$^{-/-}$ mice that were infected with increasing doses
232 of MNoV_S99 for 30 or 60 minutes (Fig. 3C). STAT1 activation increased over the course of
233 the acute infection in cells derived from WT mice. In contrast, the levels of pSTAT1 were
234 barely detectable in *Nod2*$^{-/-}$ cells at Moi 1. However, at a higher dose (Moi 5), Nod2-dependent
235 STAT1 activation was only observable at the 30 minutes time point. At 60 minutes post-
236 infection, the decrease in pSTAT1 levels in response to MNoV_S99 infection was not
237 significant anymore when compared with WT cells.
238 Next, we examined if Stat1 activation was detectable after prolonged times of infection. Indeed,
239 we measured significant differences in pStat1 expression levels between WT and *Nod2*$^{-/-}$
240 MNoV_S99-infected cells 24h post-infection at Moi 0.1 (Fig. 3D).
241 To examine whether the Mitochondrial antiviral signalling (MAVS) adaptor protein is required
242 for sensing MNoV_S99, BMDM derived from Mavs-deficient mice where compared to WT
243 cells. Interestingly, the higher pStat1 levels measured in WT cells (Moi 0.1, 1h) were
244 significantly decreased in cells derived from *Mavs*$^{-/-}$ cells (Fig. 3E).
245 Altogether, these data show a mild but significant activation of pro-inflammatory signalling
246 pathways following MNoV_S99 infection in our *in vitro* cellular models. These signalling
247 responses can be at least partially abrogated in the absence of MAVS and NOD2.
248
249 **Lower levels of inflammation in *Nod2*$^{-/-}$ mice benefit noroviral propagation**
250 MNoV_CR6 infection in DSS-induced colitis was previously shown to promote inflammation
251 in a functional Atg16l1 dependent manner[21]. Using this viral strain, we checked how loss of

252 *Nod2* influenced resolution of inflammation in response to 3% DSS treatment. As shown with
253 the S99 strain, the significantly increased inflammation levels measured by colon wall muscle
254 thickening were abrogated in *Nod2*$^{-/-}$ mice (Fig. 4A). However, a CR6 strain-specific effect can
255 be observed with these experiments since no significantly increased inflammation was
256 measured in WT mice as opposed to *Atg16l1* hypomorph mice.
257 Next, we examined the impact of the pro-inflammatory signalling activation on viral
258 propagation in these mice. In the absence of DSS induced inflammation no significant
259 differences could be found when comparing the viral load in the stool of WT, *Atg16l1*^{HM} or
260 *Nod2*$^{-/-}$ *mice (Fig. 4B)*. But, when gut epithelium tissue sections were assessed from mice
261 treated with DSS, the measured viral load was significantly increased in ileum and colon of
262 *Nod2*$^{-/-}$ mice in comparison with inflamed tissues of *Atg16l1*^{HM} mice *(Fig. 4C)*.
263 We have also analyzed the viral replication in BMDM derived from WT or *Nod2*$^{-/-}$ mice
264 infected *in vitro* with MNoV_S99 (Moi 0.1 for 24h). In that case a slight but significant increase
265 in the number of viral genomes was measured from *Nod2*$^{-/-}$ derived cultures (Fig. 4D).
266 Hence, albeit some strain effect differences between CR6 and S99, the lower levels of
267 inflammation found in *Nod2*$^{-/-}$ mice seems to favour a higher propagation of these two persistent
268 strains.
269
270 **MNoV_S99 persistence is decreased with loss of tolerance to Bacterial MDP**
271 To further explore the mechanisms behind the excessive inflammatory response associated with
272 noroviral infections we examined *Nod2* expression levels by RT-qPCR. Interestingly, they were
273 significantly increased in response to MNoV_S99 infection in Raw264.7 cells or BMDM
274 derived from WT mice (Fig. 5A and 5B).
275 This increased *Nod2* expression following norovirus infection could explain the viral-induced
276 pathogenesis that we observed in our colitis models. Indeed, with augmented NOD2 levels the

inflammatory response of myeloid cells from the lamina propria should spike up when suddenly interacting with intestinal commensal bacteria following DSS-induced epithelial abrasion.

To gain a better understanding of how these two stimuli work in tandem, we examined in our *in vitro* cellular models, Stat1 and IκBα signalling pathways activation in response to MNoV_S99 infection followed by MDP treatment. As previously shown with BMDM or Raw264.7 cells, MNoV_S99 infection did also induce Stat1 activation in monocytes isolated from WT mice (Fig. 5C and 5D, MNoV_S99+, MDP- condition). Similarly, IκBα was not activated by the viral infection alone. Though, relatively high basal levels were already detectable in mock-infected cells. As expected the treatment with the peptidoglycan MDP alone triggered potent IκBα activation without activating Stat1 (Fig. 5C, MNoV_S99-, MDP+ condition). Interestingly, while IκBα activation by single MNoV_S99 infection was not achievable, MNoV_S99 infection followed by secondary MDP treatment was associated with both pathways' moderate but significant activation (Fig. 5D, MNoV_S99+, MDP+ vs mock treated cells). In the same line of investigation, we noticed a significantly augmented pro-inflammatory cytokine TNFα response to MDP in dendritic cells that were first primed with Noroviral RNA (Fig. 5E). Next, we compared WT and *Nod2*$^{-/-}$ derived BMDM cultures' TNFα response to MNoV_S99 infection followed by MDP treatment. TNFα levels were increased with increasing doses of virus in WT cells, while they remained undetectable (Moi 0.1) or much lower (Moi 1) in *Nod2*$^{-/-}$ cells (Fig. 5F). Consequently, when noroviral replication levels were compared between Raw264.7 cells only infected with MNoV_S99 and those infected + MDP treated, viral titers measured in supernatants showed significantly decreased yields in the latter case (Fig. 5G).

Overall, these *in vitro* data fit nicely with our *in vivo* models. The increased *Nod2* transcription levels following noroviral infection in turn favours excessive inflammatory signalling pathways activation in the presence of bacterial MDP, leading ultimately to a limitation in the viral

propagation. Hence the lower inflammation in *Nod2*$^{-/-}$ mice is associated with increased propagation of MNoV_S99 and MNoV_CR6 strains.

Discussion

The breach in gut flora homeostasis termed dysbiosis is becoming central in the onset of chronic inflammatory bowel disease, such as Crohn's disease[29,30]. With the development of molecular biology techniques, alterations in the virome relevant to disease pathogenesis are thoroughly under investigation[2]. The cytosolic sensor NOD2 is very well known for its pathogen associated molecular pattern recognition activity against bacteria[13], and recently it appears it can also participate in detection of certain viruses[14]. Hence, the combination of genetic susceptibility factors and opportunistic viral infections could be one of the triggers of CD[31]. Using pro-inflammatory signalling activation downstream of NOD2 as a read-out, we have analysed if NOD2 can also participate in MNoV detection. All our *in vitro* experiments with monocytic lineage derived primary cells (e.g. BMDM, BMDC and BM) and cell line (e.g. Raw264.7) infected with different MNoV strains showed activation of the STAT1 signalling pathway implicated in the pro-inflammatory IFN response. By contrast, these responses were abrogated in *Nod2*$^{-/-}$ and *Mavs*$^{-/-}$ mice derived BMDM.

Amongst enteric viruses commonly found in the microbiota, the Norovirus is considered as a good candidate in the hypothesis of an environmental-driver in genetically susceptible hosts at the origin of Crohn's disease onset. MNoV_CR6 strain was shown to induce colitis in *Atg16l1*^{HM} mice presenting defective autophagy in a DSS colitis model[21].

Several PRR are implicated in viral sensing. MDA-5 and TLR3 have been shown to participate in detection of either MNoV_1 or CW3[11]. These are both strains which do not persist in vivo, contrary to the S99 (*Berlin)* [26] and CR6 that were used in our study.

Our *in vivo* data show significantly exacerbated inflammation when applying either 3% or 5% DSS colitis protocol to WT or *Atg16l1*^{HM} mice. The excessive MNoV-S99 or MNoV_CR6

associated inflammatory response was abrogated in *Nod2*$^{-/-}$ mice or in BMDM derived from these mice showing NOD2's implication in the pathogenesis and the viral sensing respectively. Hence, NOD2 dependent signalling adds a layer of regulation in viral sensing and finetunes the immunopathology levels caused by the infection. While in our Norovirus + DSS model knocking-down NOD2 prevents gut inflammation, it has the opposite effect with Influenza A virus (IAV) infection in the lung of *Nod2*$^{-/-}$ *or Ripk2*$^{-/-}$ mice[32]. Indeed, the NOD2-RIPK2 signalling axe has been shown to downmodulate the NLRP3 dependent mitophagy activation and the associated inflammatory response in the lung tissue of infected mice.

Noroviruses propagation or prolonged persistence is tightly regulated by the interplay between several signalling pathways. MNoV_1 replication was shown to be inhibited in macrophages following LPS mediated NF-κB activation that in turn triggers IFN-β dependent JAK-STAT antiviral activity[33]. Interestingly, in our cellular models, in addition to the phosphorylation of STAT1 that we observed when cells were infected with MNoV_S99, *Nod2* expression levels were also increased. Consequently, the subsequent treatment with MDP induced an increased NfκB signalling pathway via IκBα activation. The sequential activation of these two pro-inflammatory signalling pathways resulted in the inhibition of the MNoV_S99 propagation on one hand and the augmented production of the pro-inflammatory cytokine TNFα on the other hand. Hence, the aggravated inflammatory pathology we observed in our DSS colitis model can be explained by this NOD2-dependent signalling loop in MNoV_S99 or MNoV_CR6 infected mice. Similarly, *in vitro* the signalling and cytokine responses were NOD2 dependent since they were only observed in cultures derived from WT but not in *Nod2*$^{-/-}$ mice, at least at a lower dose (Moi 0.1) of infection. At higher doses, NOD2-independent alternative mechanisms seem to be active to promote Stat1 activation and TNFα production, but still at a lesser level than in WT cells.

In conclusion, our study shows a NOD2 dependent mechanism that prevents low level propagation of the persistent MNoV_S99 and MNoV_CR6 strains. When the noroviral infection is coupled with digestif tract injury a positive signalling loop generates a potent pro-inflammatory response that limits viral propagation.

Methods:

Unless otherwise indicated, all media and reagents were purchased from ThermoFischer Scientific.

Colitis mouse model and viral infection

All animal experiments were approved by the local ethical committee n° CEEA-2016030717519903. Age and gender related *Nod2*$^{-/-}$ and wild type littermates C57BL/6J mice (CDTA, Orléans, France) were housed 4-6 per cage, under strict pathogens-free environment. Mice were gavaged with 10^7 $TCID_{50}$PFU/mL of MNoV_S99 diluted in 200µl PBS or mock treated with PBS only. 7 days post-infection, drinking water was substituted with a 3-5% dextran sodium sulphate (DSS) (35,000-40,000 MW; TdB Consultancy) solution replaced every 2 days for a total duration of 7 days. 3% DSS colitis experiments with MNoV_CR6 were conducted as previously described in[21].

Cells and virus

Mouse leukemic monocyte macrophage cell line RAW264.7 were purchased from ECCAC (Sigma-Aldrich) and maintained in Dulbecco's modified Eagle's medium (DMEM), supplemented with 10% (*v/v*) foetal bovine serum, 1% penicillin/streptomycin and 1% sodium pyruvate.

Bone marrow derived macrophages (BMDM) were isolated from femurs of wild-type, *Nod2*$^{-/-}$ or *Mavs*$^{-/-}$ mice of C57BL/6J background [34]. Briefly, bone marrow cells were flushed out of the bones, red blood cells were lysed using a 160mM NH4CL and 170mM Tris solution for 5 minutes at RT. 3 to 6.10^6 viable cells were plated in non-cell-culture-treated petri dishes and grown for 5-7 days in Iscove's modified Dulbecco's medium (IMDM), supplemented with 10% foetal bovine serum, 1% penicillin/streptomycin, 1% non-essential amino acid, 1% sodium pyruvate, 1% glutamine, and 20% *(v/v)* conditioned-media form L929 cells.

Bone marrow derived dendritic cells were isolated similarly as BMDM cells. Then, 2.10^6 viable cells were plated in non-cell-culture-treated petri dishes and grown for 7 days in RPMI 1640, supplemented with 10% FBS, 1% P/S, 1% L-glutamine, 1% HEPES and 20% *(v/v)* conditioned-media from J558 cell line producing murine granulocyte monocyte colony stimulating factor (GM-CSF).

Monocytes were isolated from bone marrow cells by using the mouse Monocyte Isolation Kit (Miltenyi Biotec) and a QuadroMACS separator.

The MNoV-S99 strain (GenBank accession no. DQ911368) was provided by Prof. P. Maris from ANSES Fougères Laboratory (France) and was propagated in RAW 264.7 cells. MNoV-CR6 concentrated stocks were prepared as described in[35]. Briefly, supernatant from 293T cells transfected with a plasmid containing the viral genome was applied to RAW264.7 cells to amplify virus production, and virions were concentrated by ultracentrifugation and resuspension in endotoxin-free PBS. Concentration of stocks was determined by plaque assay.

For in vitro infection experiments, 3-5.10^5 viable cells were seeded in 6 wells plates. The next day, just before viral infection, cells were counted from 1 well to determine precisely the multiplicity of infection (Moi). In the remaining wells medium was removed and replaced with variable quantities of MNoV_S99 from a common viral stock in a final volume of 1 mL fresh

400 medium per well. Mock treated cells were incubated in parallel with matching quantities of
401 culture media from non-infected cells that was generated at the same time as viral stocks.
402 At various time-points after infection, supernatant was removed and cells were washed once
403 with PBS, before lysis in RIPA buffer for WB analysis or RLT buffer for total RNA extraction
404 (RNAeasy kit, Quiagen) for RT-qPCR experiments.
405
406 **Immunohistochemistry, ELISA, Western Blot, RT-qPCR and Titration**
407 For immunohistochemistry analysis, formalin-fixed colon samples were embedded in paraffin.
408 5µm sections were stained with H&E. Slides were imaged with an AxioPlan 2 (Zeiss)
409 microscope and blindly scored for inflammation severity by two investigators as previously
410 described[37].
411 For ELISA analysis, briefly 1cm colon samples were recovered from mice, luminal content was
412 flushed with PBS, samples were cut opened and resuspended over-night in 250µl DMEM
413 supplemented with 1% P/S in 24 wells plate at 37°C. The following day, supernatants were
414 collected and stored at -80°C before cytokine measurement. TNFα and Interleukin-6 proteins
415 levels were measured specifically using pre-coated 96 wells ELISA plates (R&D System)
416 following manufacturers indications.
417 For TNFα ELISA from BMDC, 5.10^5 cells were plated in 24 wells plate and treated with
418 MNoV_S99's ssRNA (extracted with RNeasy Quiagen kit) with Lipofectamine 2000[14] ± MDP
419 or MDP-DD (Invivogen) over-night and supernatants were measured for TNFα levels.
420 For TNFα ELISA from BMDM, 2.10^5 cells were plated in 96 wells plate infected with
421 MNoV_S99 (Moi 0.1 or 1) for 6h prior to MDP treatment (10ug/mL) over-night and
422 supernatants were measured for TNFα levels.
423 For western blot analysis, total proteins from cell lysates were quantified by BCA protein assay
424 kit (Pierce), equalized amounts of proteins (10-20µg) were resolved by 4-15% gradient SDS-

PAGE gels and transferred to nitrocellulose membranes. Membranes were blocked in 0,05% PBS-Tween, 5% skimmed milk solution, before incubation subsequently with primary and secondary antibodies diluted (see Table 1) in blocking solution. Following secondary antibodies incubations, signals of interest were detected using a chemiluminescence reader (ImageQuant™ Las 4000, GE Healthcare Life Sciences), images were processed and band ROI were quantified with Image J software (NCBI). Mean band intensities ± SD of protein of interest were normalized to β-actin. Relative values to control mock-infected conditions were compared between different experiments.

For *Nod2* quantification from MNoV_S99 infected BMDM or RAW264.7 cells, total RNA extraction was performed using the RNeasy Mini Kit (Qiagen). One µg of RNA was reversed transcribed in the presence of 2.5mM of oligo-dT using the Reverse Transcriptor kit (Roche) following the manufacturer's instructions. 75ng of cDNAs were amplified using Q5 High-Fidelity 2X Master Mix (New England BioLabs). Primers used in PCR amplification are available upon request.

Actb was used as an internal reference gene in order to normalize the transcript levels. Relative mRNA levels ($2^{-\Delta\Delta Ct}$) were determined by comparing (a) the PCR cycle thresholds (Ct) for *Nod2* and *Actb* (ΔCt) and (b) ΔCt values for treated and control groups (ΔΔCt).

MNoV_S99 load was determined by measuring MNoV genome copy numbers by RT-qPCR analysis as previously described[36]. Briefly, total RNA was extracted from BMDM cell cultures using the RNeasy Mini Kit (Qiagen). 5µL of RNA were used per reaction of RT-qPCR. Viral genome levels were determined using the Takyon™Dry No Rox One-Step RT Probe Mastermix (Eurogentec). Viral genomes were specifically amplified using the Fwd_5'GTGCGCAACACAGAGAAAACG3' and Rev_5'CGGGCTGAGCTTCCTGC3' primers that target MNoV ORF1 region combined to a TaqMan probe using the Stratagene Mx3005P (Agilent Technologies). The quantification of viral genome copies was obtained

using a standard curve with serial dilutions of the plasmid pMNoV1 corresponding to the full genome of MNoV1 (Dr Christiane Wobus, University of Michigan, USA). Viral load for MNoV_CR6 strain was determined by measuring genome copy numbers by RT-qPCR analysis as previously described in[21].

The net production of MNoV_S99 was determined using the $TCID_{50}$ method as described in[36]. Briefly, Raw264.7 cells were infected at Moi 1 with MNoV_S99 for 2h, before adding MDP (100ng/mL) or not in the supernatant for 24h. Titers (n = 3) were obtained from each supernatant. The net production is calculated by normalizing the amount of viruses produced with the amount of viruses used for the infection.

$NOD2^{GFP}$ immunohistochemistry imaging

$NOD2^{GFP}$ mice[38] in the C57BL/6 background were maintained at the Institut Pasteur Central Animal facility. We used heterozygous $NOD2^{GFP}$ mice since the presence of one functional copy of *NOD2* ensures that physiological responses dependent on functional NOD2 are not impaired. Heterozygous $NOD2^{GFP}$ female mice (8-12 weeks of age) were sacrificed and several centimeters of the distal ileum were removed, opened longitudinally and washed in PBS. The tissue was spread flat over a 4% *w/v* LMP agarose (Merck) pad and fixed with 4% *v/v* paraformaldehyde (VWR). The ileal tissue was then embedded in a 4% LMP agarose block and cut into 200µm-thick sections using a Microm HM 650 V Vibration microtome.

For staining, tissues were blocked, permeabilized and marked with an anti-GFP (rabbit polyclonal antibody A-11122) primary antibody and secondary Alexa Fluor 488 goat anti-rabbit antibody. Tissues sections were counter stained with DAPI (1µg/mL, BD Biosciences) and Phalloidin- iFluor 647 (1:200 dilution, Abcam and mounted using ProLong Gold Antifade reagent. Confocal acquisitions were performed using a Leica HyD SP5 confocal microscope. Image analysis was performed using Icy version 2.4.2.0[39].

References:

1. Cadwell, K. Expanding the role of the virome: commensalism in the gut. *J. Virol.* **89**, 1951–1953 (2015).
2. Norman, J. M. *et al.* Disease-specific alterations in the enteric virome in inflammatory bowel disease. *Cell* **160**, 447–460 (2015).
3. Pfeiffer, J. K. & Virgin, H. W. Viral immunity. Transkingdom control of viral infection and immunity in the mammalian intestine. *Science* **351**, aad5872 (2016).
4. Ettayebi, K. *et al.* Replication of human noroviruses in stem cell-derived human enteroids. *Science* **353**, 1387–1393 (2016).
5. Estes, M. K. *et al.* Human Norovirus Cultivation in Nontransformed Stem Cell-Derived Human Intestinal Enteroid Cultures: Success and Challenges. *Viruses* **11**, E638 (2019).
6. Ludwig-Begall, L. F., Mauroy, A. & Thiry, E. Noroviruses-The State of the Art, Nearly Fifty Years after Their Initial Discovery. *Viruses* **13**, 1541 (2021).
7. Newman, K. L. & Leon, J. S. Norovirus immunology: Of mice and mechanisms. *Eur. J. Immunol.* **45**, 2742–2757 (2015).
8. Wobus, C. E. *et al.* Replication of Norovirus in cell culture reveals a tropism for dendritic cells and macrophages. *PLoS Biol.* **2**, e432 (2004).
9. Thackray, L. B. *et al.* Murine noroviruses comprising a single genogroup exhibit biological diversity despite limited sequence divergence. *J. Virol.* **81**, 10460–10473 (2007).
10. Thorne, L. G. & Goodfellow, I. G. Norovirus gene expression and replication. *J. Gen. Virol.* **95**, 278–291 (2014).
11. McCartney, S. A. *et al.* MDA-5 recognition of a murine norovirus. *PLoS Pathog.* **4**, e1000108 (2008).
12. Wang, P. *et al.* Nlrp6 regulates intestinal antiviral innate immunity. *Science* **350**, 826–830 (2015).
13. Chamaillard, M., Girardin, S. E., Viala, J. & Philpott, D. J. Nods, Nalps and Naip: intracellular regulators of bacterial-induced inflammation. *Cell. Microbiol.* **5**, 581–592 (2003).
14. Sabbah, A. *et al.* Activation of innate immune antiviral responses by Nod2. *Nat. Immunol.* **10**, 1073–1080 (2009).
15. Kim, Y.-G. *et al.* Viral infection augments Nod1/2 signaling to potentiate lethality associated with secondary bacterial infections. *Cell Host Microbe* **9**, 496–507 (2011).
16. Karst, S. M., Wobus, C. E., Lay, M., Davidson, J. & Virgin, H. W. STAT1-dependent innate immunity to a Norwalk-like virus. *Science* **299**, 1575–1578 (2003).
17. Mumphrey, S. M. *et al.* Murine norovirus 1 infection is associated with histopathological changes in immunocompetent hosts, but clinical disease is prevented by STAT1-dependent interferon responses. *J. Virol.* **81**, 3251–3263 (2007).
18. Nice, T. J., Strong, D. W., McCune, B. T., Pohl, C. S. & Virgin, H. W. A single-amino-acid change in murine norovirus NS1/2 is sufficient for colonic tropism and persistence. *J. Virol.* **87**, 327–334 (2013).
19. Nice, T. J. *et al.* Interferon-λ cures persistent murine norovirus infection in the absence of adaptive immunity. *Science* **347**, 269–273 (2015).
20. Hwang, S. *et al.* Nondegradative role of Atg5-Atg12/ Atg16L1 autophagy protein complex in antiviral activity of interferon gamma. *Cell Host Microbe* **11**, 397–409 (2012).
21. Cadwell, K. *et al.* Virus-plus-susceptibility gene interaction determines Crohn's disease gene Atg16L1 phenotypes in intestine. *Cell* **141**, 1135–1145 (2010).

22. Travassos, L. H. *et al.* Nod1 and Nod2 direct autophagy by recruiting ATG16L1 to the plasma membrane at the site of bacterial entry. *Nat. Immunol.* **11**, 55–62 (2010).
23. Maloy, K. J. & Powrie, F. Intestinal homeostasis and its breakdown in inflammatory bowel disease. *Nature* **474**, 298–306 (2011).
24. Hugot, J. P. *et al.* Association of NOD2 leucine-rich repeat variants with susceptibility to Crohn's disease. *Nature* **411**, 599–603 (2001).
25. Hampe, J. *et al.* A genome-wide association scan of nonsynonymous SNPs identifies a susceptibility variant for Crohn disease in ATG16L1. *Nat. Genet.* **39**, 207–211 (2007).
26. Niendorf, S., Klemm, U., Mas Marques, A., Bock, C.-T. & Höhne, M. Infection with the Persistent Murine Norovirus Strain MNV-S99 Suppresses IFN-Beta Release and Activation of Stat1 In Vitro. *PloS One* **11**, e0156898 (2016).
27. Hrdý, J. *et al.* Lactobacillus reuteri 5454 and Bifidobacterium animalis ssp. lactis 5764 improve colitis while differentially impacting dendritic cells maturation and antimicrobial responses. *Sci. Rep.* **10**, 5345 (2020).
28. Wilen, C. B. *et al.* Tropism for tuft cells determines immune promotion of norovirus pathogenesis. *Science* **360**, 204–208 (2018).
29. Hold, G. L. *et al.* Role of the gut microbiota in inflammatory bowel disease pathogenesis: what have we learnt in the past 10 years? *World J. Gastroenterol.* **20**, 1192–1210 (2014).
30. Kim, D. H. & Cheon, J. H. Pathogenesis of Inflammatory Bowel Disease and Recent Advances in Biologic Therapies. *Immune Netw.* **17**, 25–40 (2017).
31. Simmons, A. Crohn's disease: Genes, viruses and microbes. *Nature* **466**, 699–700 (2010).
32. Lupfer, C. *et al.* Receptor interacting protein kinase 2–mediated mitophagy regulates inflammasome activation during virus infection. *Nat. Immunol.* **14**, 480–488 (2013).
33. Yu, P., Li, Y., Wang, Y., Peppelenbosch, M. P. & Pan, Q. Lipopolysaccharide restricts murine norovirus infection in macrophages mainly through NF-kB and JAK-STAT signaling pathway. *Virology* **546**, 109–121 (2020).
34. Michallet, M.-C. *et al.* TRADD protein is an essential component of the RIG-like helicase antiviral pathway. *Immunity* **28**, 651–661 (2008).
35. Kernbauer, E., Ding, Y. & Cadwell, K. An enteric virus can replace the beneficial function of commensal bacteria. *Nature* **516**, 94–98 (2014).
36. Hwang, S. *et al.* Murine norovirus: propagation, quantification, and genetic manipulation. *Curr. Protoc. Microbiol.* **33**, 15K.2.1-61 (2014).
37. Wirtz, S. *et al.* Chemically induced mouse models of acute and chronic intestinal inflammation. *Nat. Protoc.* **12**, 1295–1309 (2017).
38. Barreau, F. *et al.* CARD15/NOD2 is required for Peyer's patches homeostasis in mice. *PloS One* **2**, e523 (2007).
39. de Chaumont, F. *et al.* Icy: an open bioimage informatics platform for extended reproducible research. *Nat. Methods* **9**, 690–696 (2012).

Acknowledgments:

For the *NOD*^{GFP} tissue imaging, we thank the UTechS PBI, a member of the France–BioImaging infrastructure network supported by the French National Research Agency (ANR-10–INSB–04, Investissement d'Avenir program) for microscope usage and assistance. We

568 thank the members of the Institut Pasteur Central Animal Facility for their assistance with
569 animal studies. I.G.B. laboratory was supported by Investissement d'Avenir program,
570 Laboratoire d'Excellence "Integrative Biology of Emerging Infectious Diseases" (ANR-10-
571 LABX-62-IBEID), by the Investissement d'Avenir program (RHU Torino Lumière ANR-16-
572 RHUS-0008), by the French National Research Agency (ANR-16-CE15-0021) and by R&D
573 grants from Danone and MEIJI.
574 M.C. was supported by grants from the Fondation pour la Recherche Médicale
575 (DEQ20130326475) and the European Union's European Regional Development Fund. We
576 thank T. Durand and MP. Fourmaux for excellent technical assistance.
577

578 **Authors' contribution.** G.M. and M.T. performed the majority of the experimental procedures.
579 T.G. contributed to the preclinical studies in mice. M.D., T.G. and O.B. performed RT-qPCR
580 and ELISA analysis. M.D. contributed to histological analysis of colon sections. E.W.
581 performed viral genome quantification by RT-qPCR. R.W. and I.G.B. performed histological
582 analysis of tissue sections from NOD2-β-Gal reporter mice. All authors contributed to
583 interpretation of raw data and critically reviewed and/or modified the manuscript. G.M. and
584 M.C. conceived, designed and wrote the paper.
585

Figures legends:

Figure 1: MNoV_S99 aggravates inflammation in DSS-induced colitis
A)- In vivo experimental design, C57BL/6J mice were orally gavaged with PBS or MNoV_S99 (10^7 $TCID_{50}$PFU/mL), 7 days later, all the mice were given DSS in drinking water for a week. Mice were weighed daily for weight loss comparison. **B)-** 3% DSS-induced colitis ± MNoV_S99 (n = 6). **C)-** 5% DSS-induced colitis ± MNoV_S99 (n = 6). In B) and C), statistical differences were determined by 2 ways ANOVA test, * $p < 0.05$, ** $p < 0.01$, *** $p < 0.001$. **D)-** Representative images from H&E staining of colon sections from mock-treated (Control) or 3% DSS ± MNoV_S99 treated mice. Insets showing higher magnifications from each image are presented next to each image. **E)-** Muscle wall thickness was determined with Image J from colon section images. Percentages of increase are plotted after baseline subtraction relatively to the values obtained from Control mice (n = 6). **F)-** Histological intestinal epithelial inflammation scores comparison between Control, 3% or 5% DSS ± MNoV_S99 treated mice (n = 6). **G)-** Colon length comparison between Control and 5% DSS ± MNoV_S99 treated mice **H-** IL6 secretion levels from colon explants from mock or 5% DSS ± MNoV_S99 treated mice (n = 6). Statistical differences were determined with Student's t-Test in E, F, G and H.

Figure 2: MNoV_S99 associated inflammation is NOD2 dependent
Weight loss comparison in **A)-** 3% DSS-induced colitis ± MNoV_S99 in WT mice (n=6) and **B)-** in *Nod2*$^{-/-}$ mice (n=6), statistical differences were determined by 2 ways ANOVA test, * $p < 0,05$, ** $p < 0,01$, *** $p < 0,001$. **C)-** Representative images of H&E staining of colon sections from mice in A) and B). Insets showing higher magnifications are presented below each image. **D)-** Percentages of increase of muscle wall thickness from colon section images are plotted after baseline subtraction relatively to the values obtained from WT mice treated only with DSS (n = 6), statistical differences were determined with Student's t-Test.

Figure 3: MNoV_S99 associated pro-inflammatory signalling is NOD2 and MAVS-dependent in myeloid lineage cells
A)- Representative image showing an intestinal villus from a *Nod2*^{GFP} mouse (GFP is shown in green, Phalloidin in grey and DAPI in blue); scale bare represents 50µm. **B)-** Representative western blot showing STAT1 signalling pathway activation after 1h infection (Moi 1) with the mentioned MNoV strains in BMDM. Below are shown quantification of pSTAT1 bands intensities normalized to β-actin and relative to mock-infected cells (n = 3, mean ± SEM), statistical differences were determined by 1 way ANOVA test * $p < 0,05$, ** $p < 0,005$. **C)-** STAT1 activation in response to MNoV_S99 (Moi 1 or 5) in BMDM from WT vs *Nod2*$^{-/-}$ infected for 30 or 60 minutes. The lower panel shows quantification of pSTAT1, bands intensities normalized to β-actin and relative to mock-infected cells (n = 3, mean ± SEM). Statistical differences were determined by 2 ways ANOVA test * $p < 0,05$. **D)-** STAT1 activation in response to MNoV_S99 (Moi 0.1) in WT or *Nod2*$^{-/-}$ BMDM infected for 24h. Relative quantification of pSTAT1 (n = 3, mean ± SEM) is shown in the lower panel, statistical differences were determined by 2 ways ANOVA test *** $p < 0,0005$. **E)-** STAT1 activation in response to MNoV_S99 (Moi 0.1) in BMDM from WT vs *Mavs*$^{-/-}$ infected for 60 minutes. Relative quantification of pSTAT1 (n = 4, mean ± SEM) are shown below. The lower panel shows the mock vs Moi 0.1 infected cells quantification of pSTAT1. Statistical differences were determined by 2 ways ANOVA test * $p < 0,05$.

Figure 4: NOD2 dependent noroviral load
A)- WT, *Nod2*$^{-/-}$ and *Atg16l1*^{HM} mice (n = 5 each) were treated with 3% DSS and infected with MNoV_CR6 (3.10^7 PFU). Inflammation was measured as percentage of increase in muscle thickness at the anal-rectal junction in colonic section images plotted after baseline subtraction relatively to the values obtained from WT mice. **B)-** The viral load measured in stools from WT, *Nod2*$^{-/-}$ and *Atg16l1*^{HM} mice at day 3, 5 and 7 post-infection with MNoV_CR6 (3.10^7 PFU) (n = 8). **C)-** The viral load measured

from indicated tissue samples from MNoV_CR6 infected (3.10^7 PFU) WT, *Nod2*$^{-/-}$ and *Atg16l1*^{HM} mice that were treated for 1 week with D55 3% (n = 5). **D)-** MNoV_S99 genome quantification from WT and *Nod2*$^{-/-}$ BMDM cells infected with MNoV_S99 (Moi 0.1 for 24h) (n = 3). All the statistical differences were measured with Student's t-Test.

Figure 5: NOD2 dependent pro-inflammatory signalling associated with MNoV_S99 infection and bacterial MDP

Quantification of *Nod2* mRNA levels measured by RT-qPCR in **A)-** in Raw264.7 cells infected with MNoV_S99 (Moi 0.1 or 1, for 24h) and in **B)-** in BMDM from WT mice (Moi 0.1, for 24h) normalized to *ActB* and relative to mock-infected cells (n = 3). **C)-** Representative western blot showing STAT1 and IκBα signalling pathways modulation in cell lysates from monocytes that were either infected with MNoV_S99 (Moi 5, 2h), treated with MDP (10ng/mL, 2h), or a combination of both. **D)-** Quantification and comparison of pSTAT1 and pIκBα signals between MNoV_S99 infected alone cells or in combination with MDP (10ng/mL, 2h), (n = 3), with the band intensity being normalized to β-actin and relative to mock-treated cells. **E)** TNFα production by BMDC subjected to MNoV_S99's ssRNA (10µg/mL) alone, or supplemented with either MDP (1µg/mL) or MDP-DD (1µg/mL) overnight. **F)** TNFα production by BMDM cells infected with MNoV_S99 (Moi 0.1 or 1) for 6h, prior to being treated with MDP (10µg/mL) overnight. **G)** Net production of MNoV_S99 in Raw264.7 cells infected with MNoV_S99 (Moi 1 for 2h before MDP treatment (100ng/mL) for 24h). Statistical differences were analyzed with Student's t Test.

Supplementary Figures

Supplementary Figure 1: Analysis of MNoV_S99 associated NOD2 dependent inflammation measurements from mice showed in Figure 2

A) Colon length comparison between WT and *Nod2*$^{-/-}$ from 3% DSS ± MNoV_S99 treated mice, statistical differences were determined with Student's t-Test, * p <0,02. **B)-** Histological scores comparison between WT and *Nod2*$^{-/-}$ ± MNoV_S99 treated mice, statistical differences were determined with Student's t-Test, * p <0,05. **C)-** TNFα production of explants (ON) from WT and *Nod2*$^{-/-}$ 3% DSS ± MNoV_S99 treated mice was measured by ELISA.

Supplementary Figure 2: MNoV_S99 associated pro-inflammatory signalling pathways activation

Representative western blot showing STAT1, IκBα, AKT and ERK signalling pathways' modulation in cell lysates from Raw264.7 that were either infected with MNoV_S99 (Moi 1) for various times or mock treated for 60 min. β-actin was used as loading control.

Tables:

Table1: Antibodies used for Western Blotting		
Primary antibodies	Dilution	Supplier
anti-phosphoStat1 (Tyr 701) (58D6) (85kDa)	1/1000	Cell Signaling Technology
anti-Stat1(D1K9Y)(85kDa)	1/1000	
anti-phosphoIκBα (Ser32/36) (5A5) (40kDa)	1/1000	
anti-IκBα (44D4) (39kDa)	1/1000	
anti-phosphoAKT (Ser473) (D9E) (60kDa)	1/1000	
anti-AKT (60kDa)	1/1000	
anti-phospho44/42 MAPK (Erk1/2) (Trh202/Tyr204) (197G2) (42, 44 kDa)	1/1000	
anti-p44/42 (Erk1/2) (42, 44 kDa)	1/1000	
anti-βactin (45kDa)	1/500	
Secondary antibodies	Dilution	Supplier
anti-Rabbit_HRP (#711-035-152)	1/5000	Jackson Laboratories
anti-Mouse_HRP (#115-005-003)	1/5000	

Figure 1

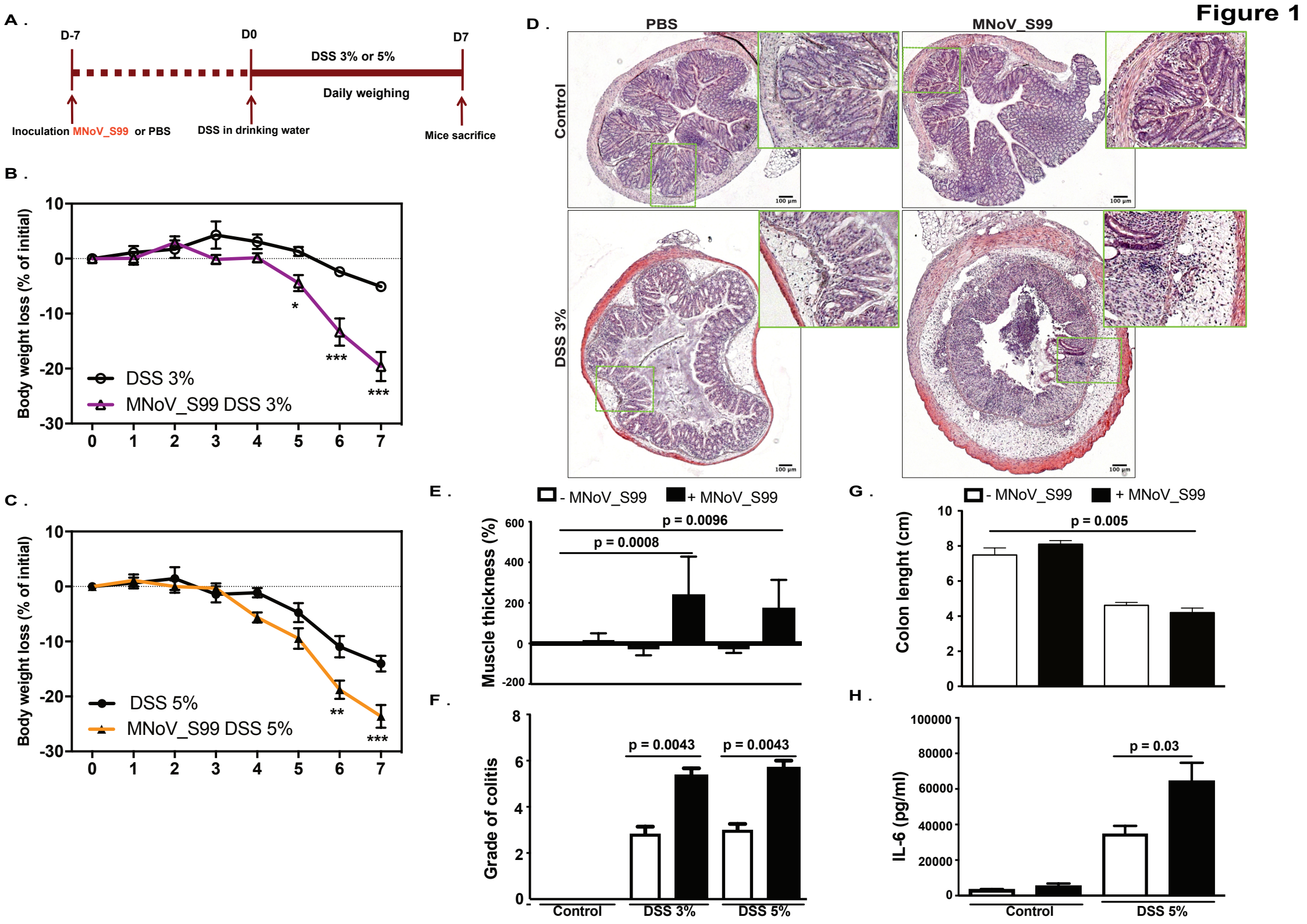
A .
D-7
D0
D7
DSS 3% or 5%
Daily weighing
Inoculation MNoV_S99 or PBS
DSS in drinking water
Mice sacrifice
B .
Body weight loss (% of initial)
DSS 3%
MNoV_S99 DSS 3%
C .
Body weight loss (% of initial)
DSS 5%
MNoV_S99 DSS 5%
D .
PBS
MNoV_S99
Control
DSS 3%
100 µm
E .
- MNoV_S99
+ MNoV_S99
Muscle thickness (%)
p = 0.0096
p = 0.0008
F .
Grade of colitis
p = 0.0043
p = 0.0043
Control
DSS 3%
DSS 5%
G .
- MNoV_S99
+ MNoV_S99
Colon lenght (cm)
p = 0.005
H .
IL-6 (pg/ml)
p = 0.03
Control
DSS 5%

Figure 2

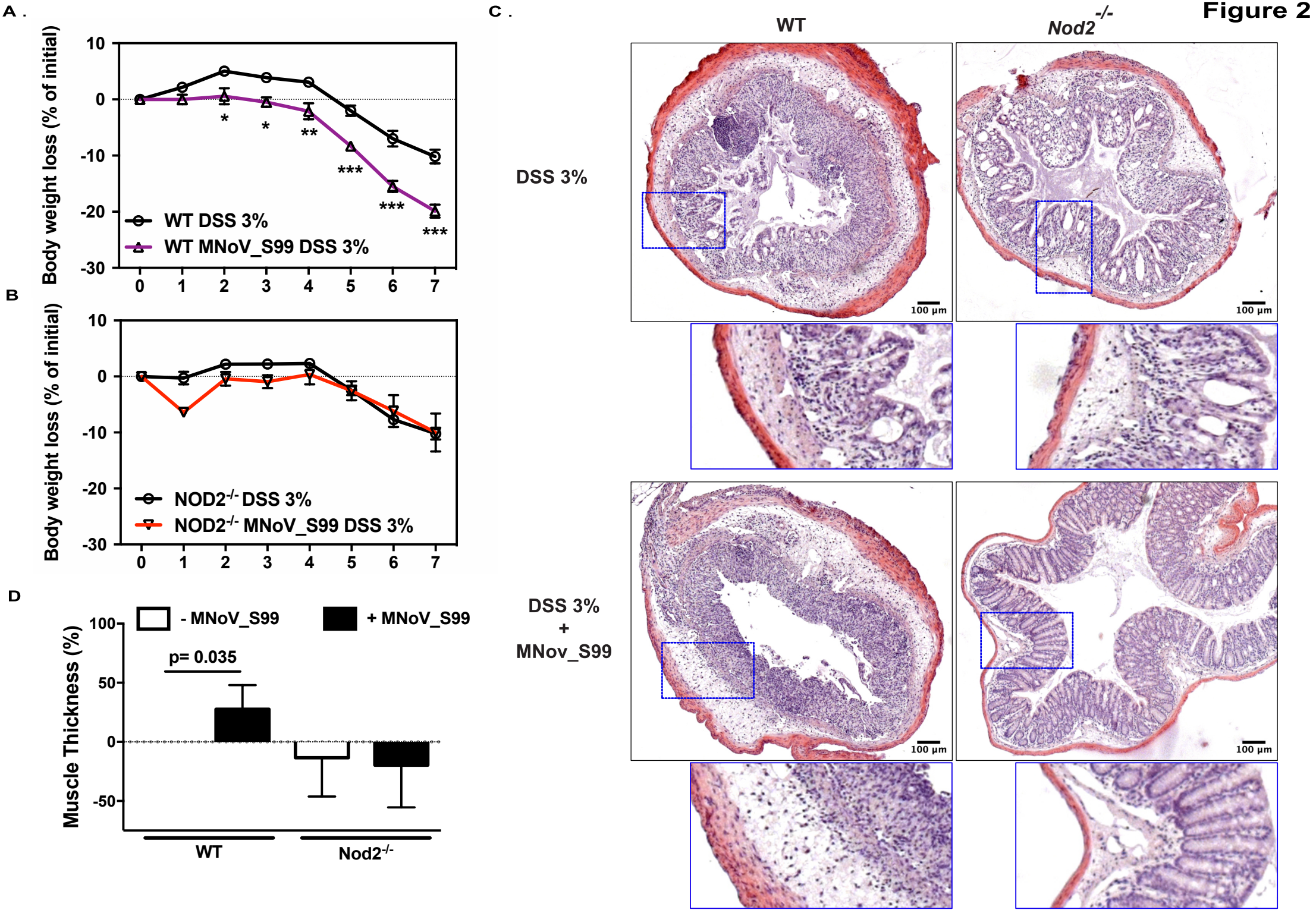
A.
Body weight loss (% of initial)
10
0
-10
-20
-30
0 1 2 3 4 5 6 7
*
*
**
***
***
***
WT DSS 3%
WT MNoV_S99 DSS 3%
B
Body weight loss (% of initial)
NOD2-/- DSS 3%
NOD2-/- MNoV_S99 DSS 3%
C.
WT
Nod2-/-
DSS 3%
DSS 3%
+
MNov_S99
100 µm
D
- MNoV_S99
+ MNoV_S99
Muscle Thickness (%)
100
50
0
-50
p= 0.035
WT
Nod2-/-

Figure 3

A .

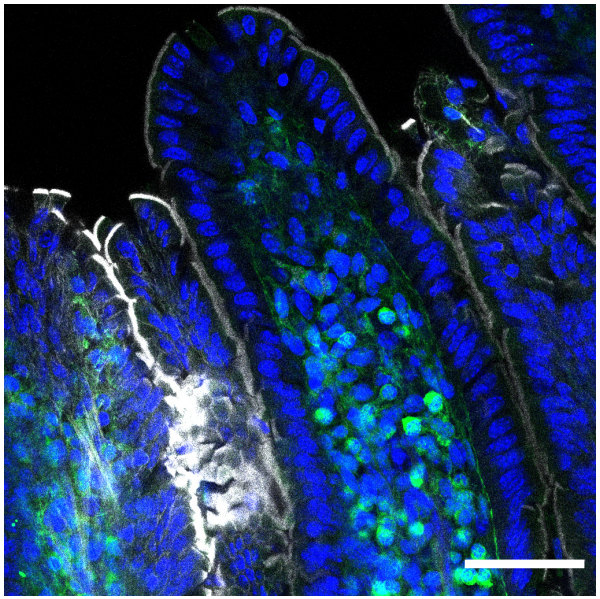

B .

C .

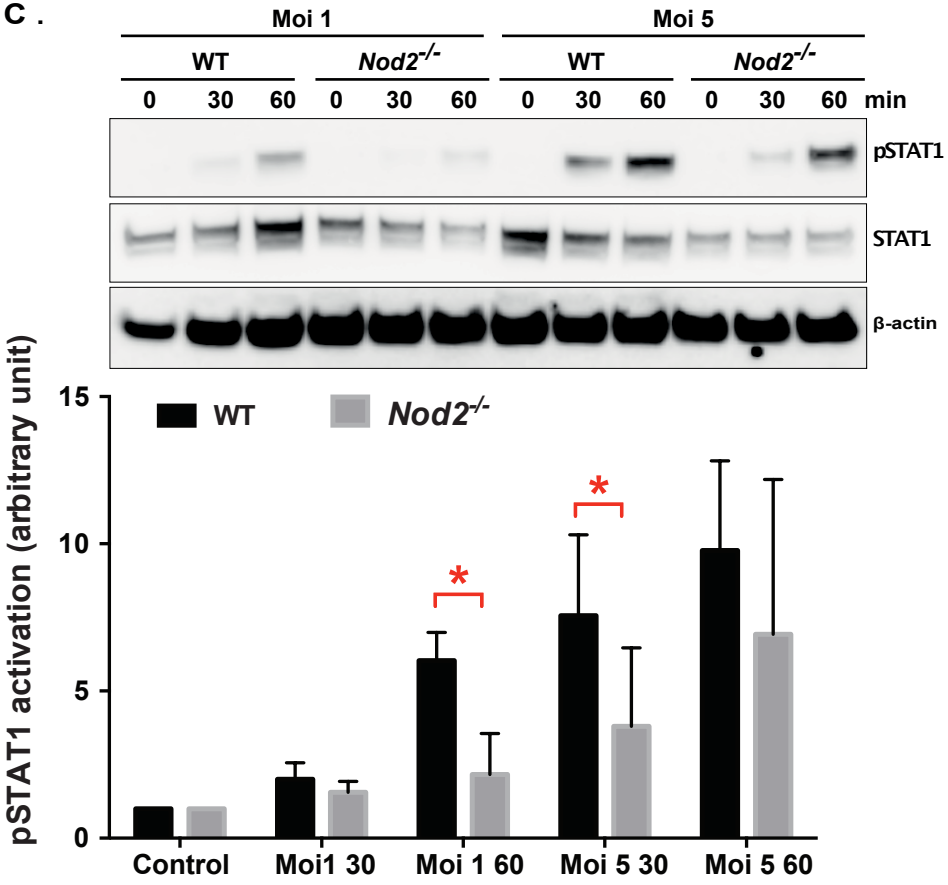

D .

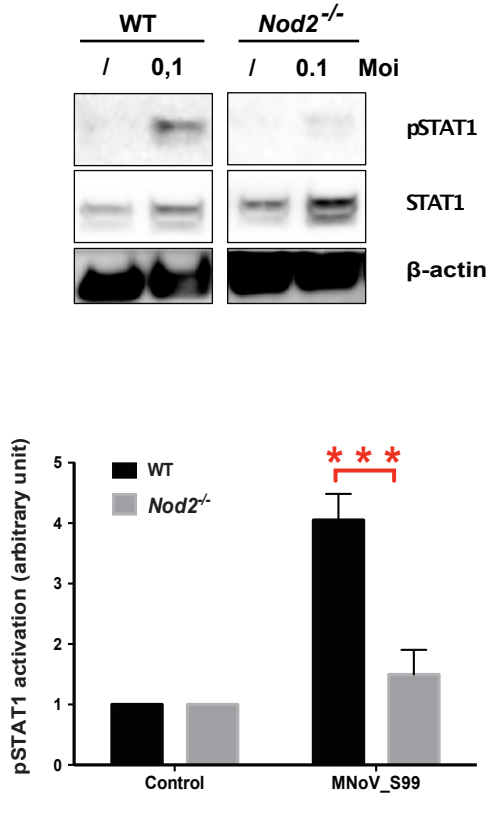

E .

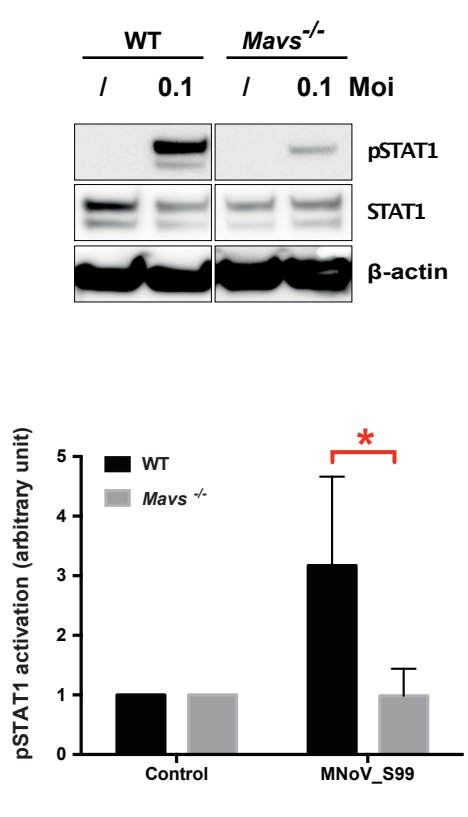

Figure 4

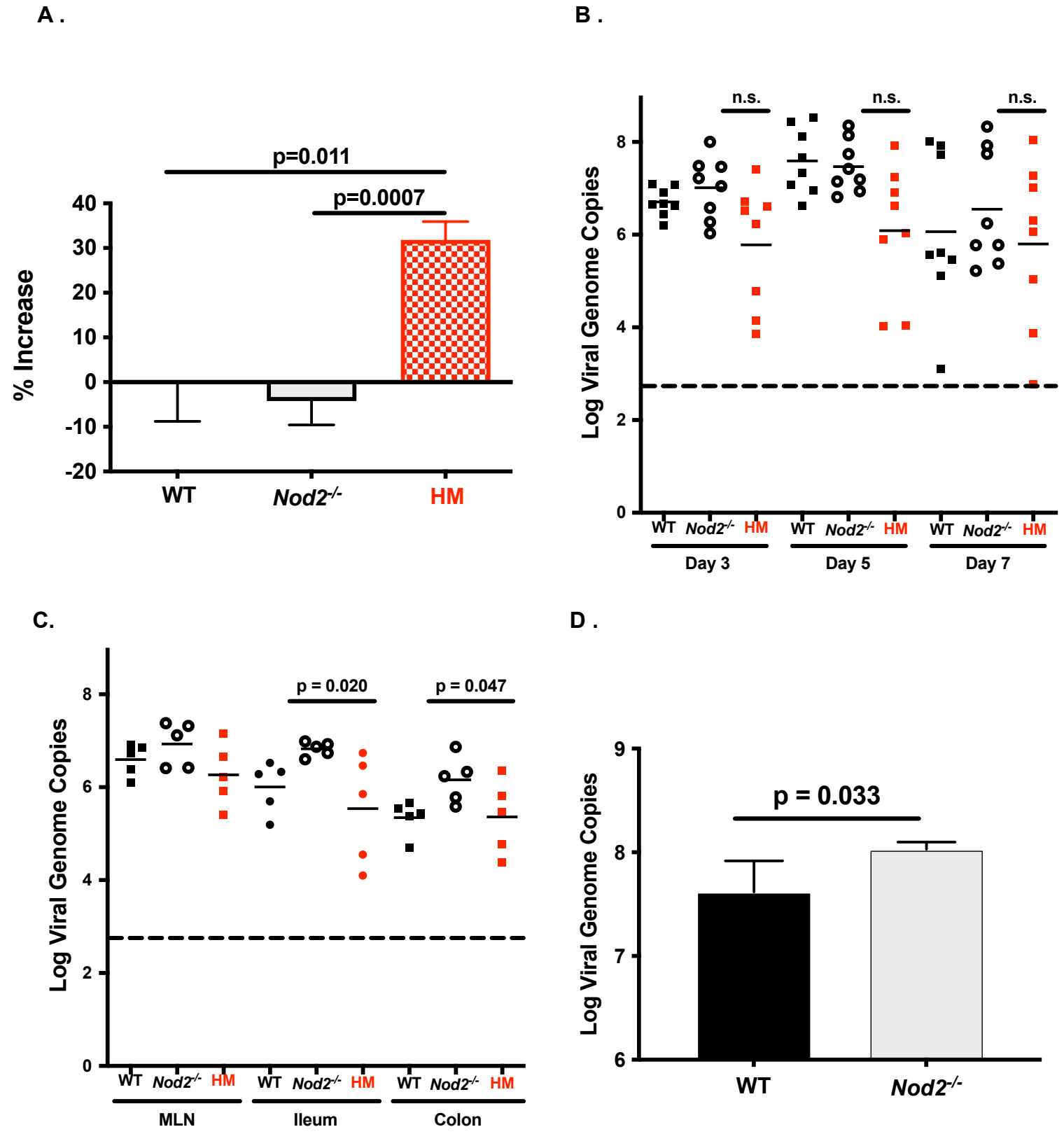
A .
p=0.011
p=0.0007
% Increase
40
30
20
10
0
-10
-20
WT
Nod2-/-
HM
B .
n.s.
n.s.
n.s.
Log Viral Genome Copies
8
6
4
2
0
WT
Nod2-/-
HM
Day 3
Day 5
Day 7
C.
p = 0.020
p = 0.047
Log Viral Genome Copies
8
6
4
2
0
MLN
Ileum
Colon
D .
p = 0.033
Log Viral Genome Copies
9
8
7
6
WT
Nod2-/-

Figure 5

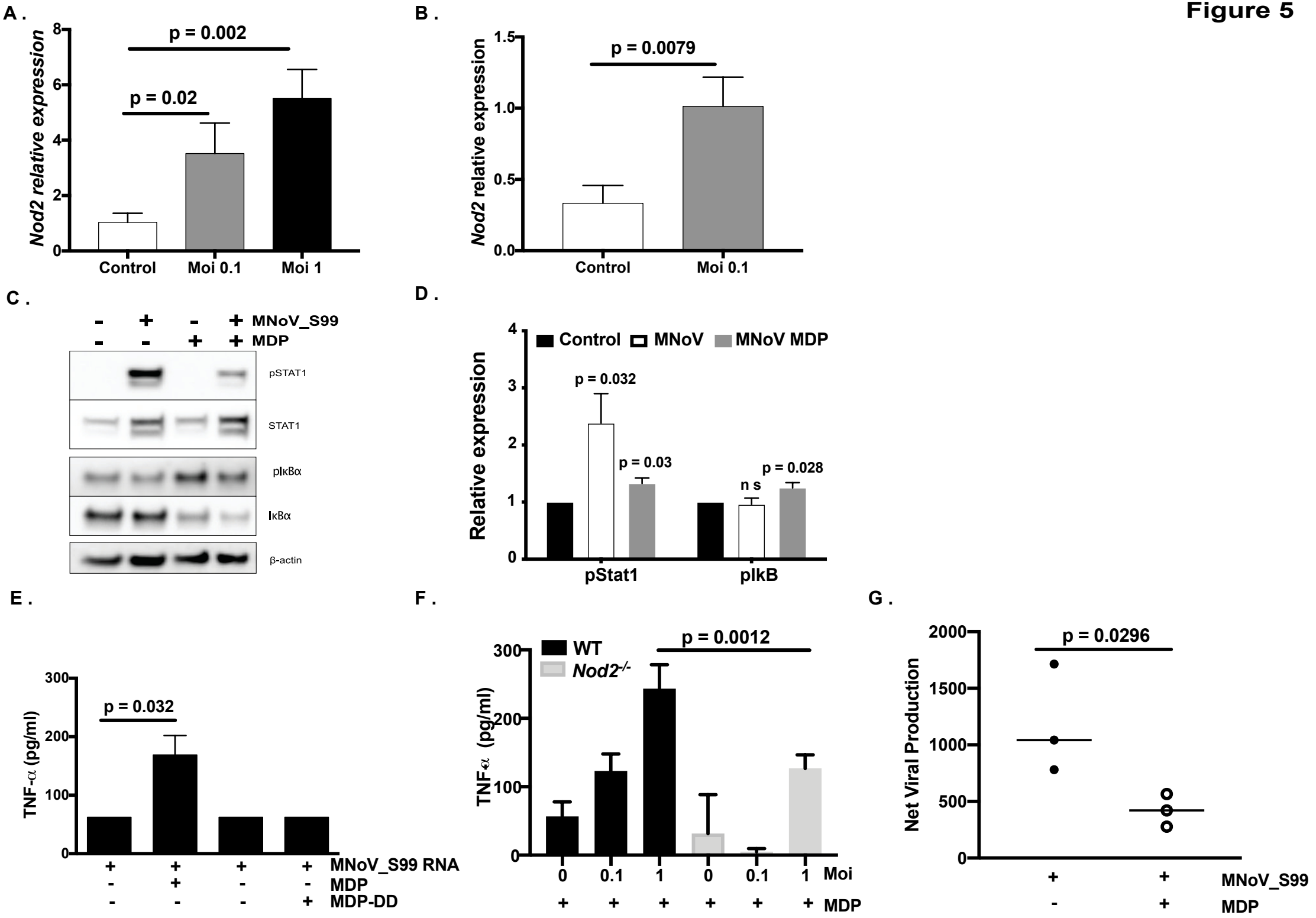
A.
Nod2 relative expression
p = 0.002
p = 0.02
Control
Moi 0.1
Moi 1
B.
Nod2 relative expression
p = 0.0079
Control
Moi 0.1
C.
MNoV_S99
MDP
pSTAT1
STAT1
pIκBα
IκBα
β-actin
D.
Control
MNoV
MNoV MDP
Relative expression
p = 0.032
p = 0.03
n s
p = 0.028
pStat1
pIkB
E.
TNF-α (pg/ml)
p = 0.032
MNoV_S99 RNA
MDP
MDP-DD
F.
WT
Nod2-/-
TNF-α (pg/ml)
p = 0.0012
Moi
MDP
G.
Net Viral Production
p = 0.0296
MNoV_S99
MDP

Figure S1

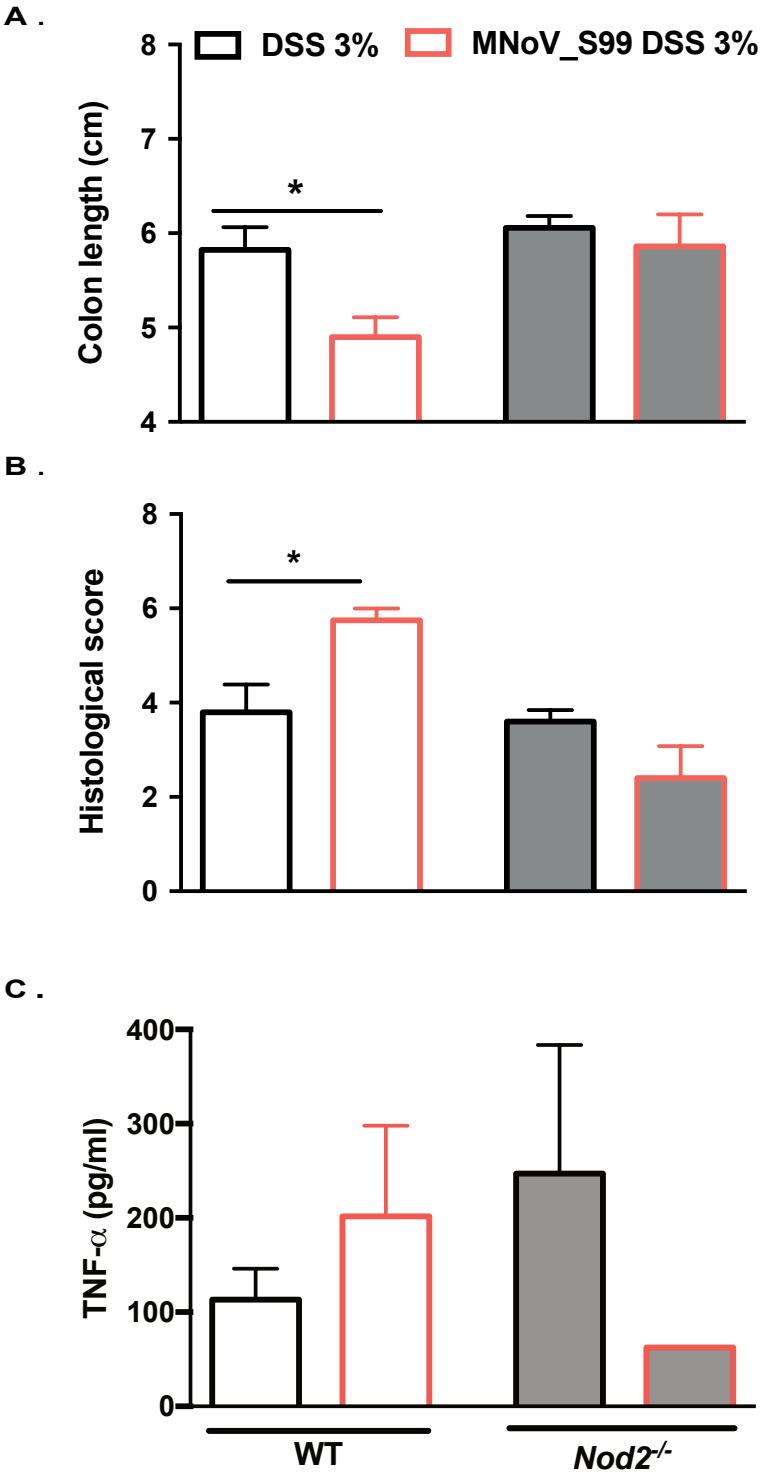
A .
DSS 3%
MNoV_S99 DSS 3%
Colon length (cm)
8
7
6
5
4
*
B .
Histological score
8
6
4
2
0
*
C .
TNF-α (pg/ml)
400
300
200
100
0
WT
Nod2-/-

Figure S2

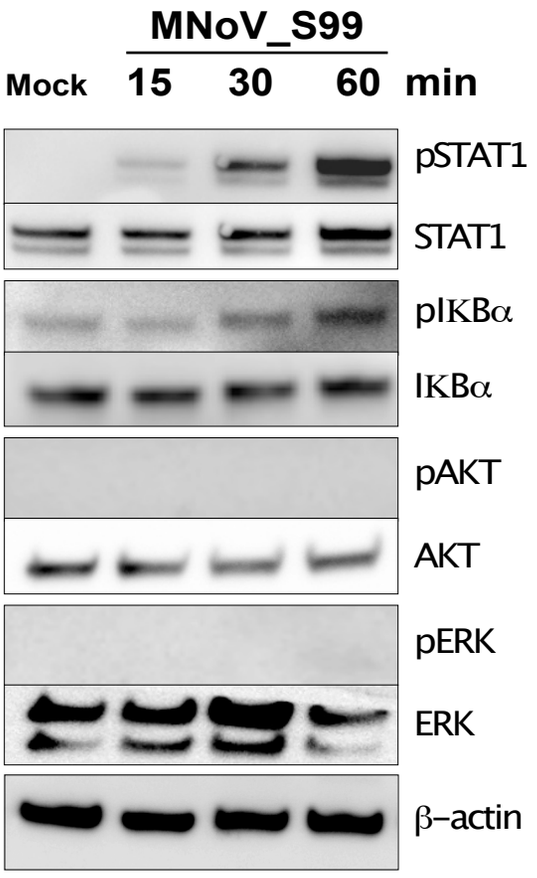
MNoV_S99
Mock
15
30
60
min
pSTAT1
STAT1
pIKBα
IKBα
pAKT
AKT
pERK
ERK
β–actin